

ExoGemS Detection of a Metal Hydride in an Exoplanet Atmosphere at High Spectral Resolution

LAURA FLAGG,¹ JAKE D. TURNER,^{1,2} EMILY DEIBERT,³ ANDREW RIDDEN-HARPER,⁴
ERNST DE MOOIJ,⁵ RYAN J. MACDONALD,^{6,1,2} RAY JAYAWARDHANA,⁷ NEALE GIBSON,⁸
ADAM LANGEVELD,¹ AND DAVID SING⁹

¹*Department of Astronomy and Carl Sagan Institute, Cornell University, Ithaca, New York 14853, USA*

²*NHFP Sagan Fellow*

³*Gemini Observatory, NSF's NOIRLab, Casilla 603, La Serena, Chile*

⁴*Las Cumbres Observatory, 6740 Cortona Drive, Suite 102, Goleta, CA 93117, USA*

⁵*Astrophysics Research Centre, School of Mathematics and Physics, Queen's University Belfast, University Road,
Belfast BT7 1NN, United Kingdom*

⁶*Department of Astronomy, University of Michigan, Ann Arbor, MI 48109, USA*

⁷*Department of Astronomy, Cornell University, Ithaca, New York 14853, USA*

⁸*School of Physics, Trinity College Dublin, The University of Dublin, Dublin 2, Ireland*

⁹*Department of Earth & Planetary Sciences, Johns Hopkins University, Baltimore, MD, 21218, USA*

ABSTRACT

Exoplanet atmosphere studies are often enriched by synergies with brown dwarf analogs. However, many key molecules commonly seen in brown dwarfs have yet to be confirmed in exoplanet atmospheres. An important example is chromium hydride (CrH), which is often used to probe atmospheric temperatures and classify brown dwarfs into spectral types. Recently, tentative evidence for CrH was reported in the low-resolution transmission spectrum of the hot Jupiter WASP-31b. Here, we present high spectral resolution observations of WASP-31b's transmission spectrum from GRACES/Gemini North and UVES/VLT. We detect CrH at 5.6σ confidence, representing the first metal hydride detection in an exoplanet atmosphere at high spectral resolution. Our findings constitute a critical step in understanding the role of metal hydrides in exoplanet atmospheres.

Keywords: Exoplanet atmospheres (487) — Planetary atmospheres (1244) — Exoplanets (498) — Exoplanet atmospheric composition (2021)

1. INTRODUCTION

Metal hydrides and metal oxides have been used to characterize the atmospheres of very

cool stars and brown dwarfs for decades. TiO is useful for classifying stars as warm as ~ 4000 K (Reid et al. 1995), while metal hydrides like FeH and CrH become the primary tools for determining the temperatures of brown dwarfs with $T_{\text{eff}} \lesssim 2500$ K when using optical spectra (Kirkpatrick et al. 1999; Martín et al. 1999). CrH is

Corresponding author: Laura Flagg
laura.s.flagg@gmail.com

also a sensitive probe of rainout chemistry and disequilibrium atmospheric dynamics in brown dwarfs (Burrows et al. 2002).

Many hot giant exoplanets share similar temperatures to brown dwarfs, so metal oxides and hydrides could also sculpt exoplanet spectra and drive thermal inversions (Fortney et al. 2008; Gandhi & Madhusudhan 2019). However, searches for TiO and VO have had limited success, with initial detections often challenged by subsequent observations (e.g. Nugroho et al. 2017; Herman et al. 2020). There is no consensus on the reason for the lack of detections. Chemical equilibrium models indicate that, as with brown dwarfs, molecules such as CrH and FeH should have significant abundances in exoplanet atmospheres from ~ 1200 – 2000 K (e.g. Visscher et al. 2010).

Observational evidence for metal hydrides in exoplanet atmospheres has been tentatively reported from low spectral resolution transmission spectra for a handful of planets. Evidence of FeH has been reported in WASP-79b’s Hubble Space Telescope (HST) WFC3 transmission spectrum (Sotzen et al. 2020; Skaf et al. 2020), though subsequent observations with HST’s STIS instrument favored unocculted stellar faculae with no FeH (Rathcke et al. 2021). Hints of CrH have been inferred for the warm Neptune HAT-P-26b (MacDonald & Madhusudhan 2019) and the hot Jupiter WASP-31b (Braam et al. 2021). However, the low spectral resolution observations underpinning these inferences render the robust identification of a chemical species challenging, since bands from alternative molecules can often be hard to distinguish.

High-resolution spectroscopy offers a promising avenue to search for metal hydrides in giant exoplanet atmospheres. Since absorption lines from individual molecules are resolved at high resolution, specific molecules can be robustly and directly detected. To date, the only attempt to detect metal hydrides at high spectral

resolution was by Kesseli et al. (2020), who surveyed 12 planets and reported no evidence for FeH. The definitive detection of metal hydrides would be an important advancement in our understanding of hot giant planet atmospheres, unveiling their role in driving the thermal structure of hot giant planet atmospheres.

In this letter, we report the detection of CrH at high spectral resolution in the atmosphere of WASP-31b. We present high-resolution spectra from both the ExoGemS survey with Gemini-North/GRACES and VLT/UVES, both of which establish the presence of CrH with a combined significance of $>5\sigma$. This marks the first detection of a metal hydride from a high-resolution exoplanet spectrum.

2. WASP-31B

The hot Jupiter WASP-31b, discovered by Anderson et al. (2011), orbits an F5 star on a 3.4 day orbit. (See Table 1 for the full parameters of the system used in this paper). At $0.5 M_J$ and $1.5 R_J$ (Anderson et al. 2011), it is has extremely low-density, even for a giant planet; its equilibrium temperature is ~ 1400 K (Braam et al. 2021). Brown et al. (2012) used the Rossiter-McLaughlin effect to measure the alignment of the orbit with the rotation of WASP-31: they found $\lambda = 2.8 \pm 3.4$ degrees, implying the system is very well aligned.

2.1. *The Atmosphere of WASP-31b*

Sing et al. (2015) used HST and Spitzer to probe the atmosphere between 0.3 and $1.7 \mu\text{m}$. In the optical, they found no Na, but evidence of K at a 4.2σ confidence level. The expected H₂O feature in the infrared was also undetected, implying the presence of clouds. Several papers have reanalyzed the HST data and reported fairly similar results (Barstow et al. 2017; Welbanks et al. 2019). MacDonald & Madhusud-

Table 1. Orbital and physical parameters of the WASP-31 system used in this analysis.

Parameter	Symbol (Unit)	Value	Reference
Stellar mass	M_* (M_\odot)	1.15 ± 0.08	Anderson et al. (2011)
Projected stellar rotational velocity	$v \sin i$ (km/s)	7.9 ± 0.6	Anderson et al. (2011)
Magnitude	V (mag)	11.90 ± 0.02	Zacharias et al. (2013)
Orbital period	P (days)	3.4058864 ± 0.0000018	this paper
Epoch of mid-transit	t_c (BJD)	2455873.8673 ± 0.0017	this paper
Transit duration	T_{14} (hours)	2.6472 ± 0.0312	Anderson et al. (2011)
Planetary radius	R_p (R_J)	1.549 ± 0.050	Anderson et al. (2011)
Planetary mass	M_p (M_J)	0.478 ± 0.029	Anderson et al. (2011)
Equilibrium Temperature	T_{eq} (K)	1393	Braam et al. (2021)
Inclination	i (degrees)	$84.41^{+0.22}_{-0.22}$	Anderson et al. (2011)
Systemic velocity	γ_{sys} (km/s)	-0.34 ± 2.07	Gaia Collaboration et al. (2018)
Stellar radial velocity semi-amplitude	k_* (m/s)	$59.4^{+0.28}_{-0.29}$	Bonomo et al. (2017)
Planetary radial velocity semi-amplitude	k_p (km/s)	148.0 ± 14.8	this paper
Linear limb darkening coefficient	u_1	0.2387	Claret (2017)
Quadratic limb darkening coefficient	u_2	0.3118	Claret (2017)

han (2017) noted weak evidence for NH_3 using HST-WFC3 data.

Gibson et al. (2017) used VLT/FORS2 to characterize the atmosphere during transit. They confirmed the cloud deck seen by Sing et al. (2015), but saw no evidence for K. Gibson et al. (2019) followed up with observations using VLT/UVES, and did not find evidence of K either. McGruder et al. (2020) reported the same, using IMACS on Magellan.

Braam et al. (2021) reanalyzed the HST data from Sing et al. (2015). They found significant — albeit inconclusive — evidence for not only H_2O but also CrH, the latter of which has no confirmed detections in any exoplanet.

3. OBSERVATIONS

We observed one transit of WASP-31b on 2022-March-12 as part of the Exoplanets with Gemini Spectroscopy (ExoGemS) survey. ExoGemS uses GRACES (Gemini Remote Access to CFHT ESPaDOnS Spectrograph) on Gemini-North to observe a large

sample of exoplanets with transmission spectroscopy. GRACES covers from 400 to 1050 nm at $R \sim 66,000$.

141 spectra were acquired between 09:17 and 13:21 UTC, corresponding to airmasses between 1.28 and 1.94, for an expected transit between 10:36 and 13:11 UTC. In the order with the most prominent CrH band, ~ 860 nm, the SNR ranged from 32 to 85. There was a drop in SNR around the time of mid-transit, with spectra before mid-transit having an average SNR of 65 and spectra after having an average SNR of 41. One order of the reduced spectra is plotted in the top panel of Figure 1.

The GRACES data was supplemented by archival VLT/UVES data of two WASP-31b transits, taken in the spring of 2017 and published by Gibson et al. (2019). As that data were not intended to look for CrH, the chosen wavelength range ends at 866 nm and only overlaps with the strongest CrH band, which starts at 860 nm, for ~ 6 nm.

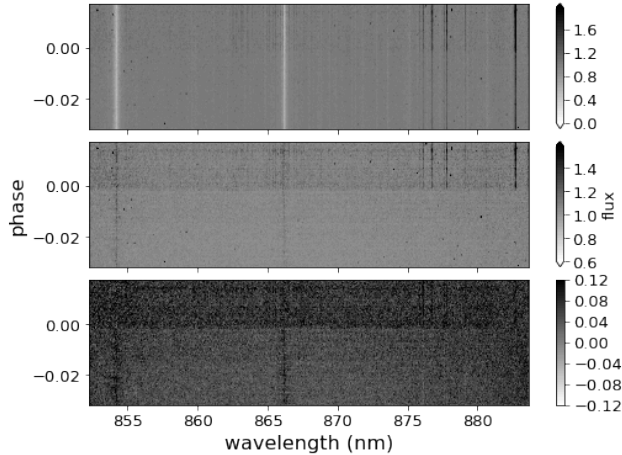


Figure 1. One order of the reduced spectra from GRACES (top), with the main stellar and telluric signal divided out (middle), and after SVD processing (bottom).

4. METHODS

4.1. Calculation of the Transit Ephemeris

To update the transit ephemeris we analyzed the publicly available TESS data. TESS observed WASP-31b in Sectors 9 (2019-02-28 to 2019-03-26, [doi:10.17909/yk3b-g272](https://doi.org/10.17909/yk3b-g272)) and 36 (2021-03-07 to 2021-04-02, [doi:10.17909/x636-7g89](https://doi.org/10.17909/x636-7g89)). We use the Data Validation Timeseries light curves because they have less scatter in their out-of-transit (OoT) baseline. We followed the same procedure as in [Turner et al. \(2021, 2022\)](#) to model the light curves and determine the transit ephemeris.

We modeled the TESS transits of WASP-31b with the EXOplanet MODELing Package (EXOMOP; [Pearson et al. 2014](#); [Turner et al. 2017](#))¹ to find a best-fit. EXOMOP creates a model transit using the analytic equations of [Mandel & Agol \(2002\)](#) and the data are modeled using a Differential Evolution Markov Chain Monte Carlo (DE-MCMC; [Eastman et al. 2013](#)) analysis and uses the residual permutation, time-averaging, and wavelet methods to account for red noise. Each TESS transit was mod-

eled with EXOMOP independently. We used 20⁶ links and 20 chains for the DE-MCMC model and use the Gelman-Rubin statistic ([Gelman & Rubin 1992](#)) to ensure chain convergence ([Ford 2006](#)). The mid-transit time (t_c), scaled semi-major axis (a/R_*), planet-to-star radius (R_p/R_*), and inclination (i) are set as free parameters for every transit. The linear and quadratic limb darkening coefficients and period are fixed during the analysis. The linear and quadratic limb darkening coefficients are taken from [Claret \(2017\)](#) and are set to 0.2387 and 0.3118, respectively. We find an updated period of 3.4058864 ± 0.0000018 days and a mid-transit ($t_c[0]$) of 2455873.8673 ± 0.0017 BJD_{TDB} using the TESS observations (see [Table A1](#) for the individual TESS mid-transit times).

4.2. Removal of Stellar and Telluric Signal

As in [Deibert et al. \(2021\)](#), the ExoGemS spectra were reduced with the OPERA pipeline ([Martoli et al. 2012](#)), designed for ESPaDOnS data, which extracts the spectra, calibrates the wavelength solution, and removes the blaze function. The UVES spectra were reduced in the manner of [Gibson et al. \(2019\)](#). After the spectral extraction, we used the same procedure for both data sets for consistency.

The basic procedure for removing the stellar and telluric features relies on the fact that they are essentially stationary in time, while the planet’s signal is moving in Doppler space (e.g [Brogi et al. 2013](#); [Lockwood et al. 2014](#); [Flagg et al. 2019](#)). For example, over the course of the GRACES observations, the planet’s signal shifts 45 km/s. The specific procedure used for this paper is a custom code.² We first put all spectra onto a common wavelength grid that is evenly spaced in velocity. We then divided by the median out-of-transit spectrum to remove the blaze function and the basic spec-

¹ EXOMOPv7.0; <https://github.com/astrojake/EXOMOP>

² https://github.com/lauraflagg/svd_exoplanets

tral features. We further removed the stellar and telluric features using singular value decomposition (SVD) as in [Line et al. \(2021\)](#). For GRACES, we used 4 components; for UVES we used 6. The number of components was chosen using the Δ CCF method (e.g. [Spring et al. 2022](#); [Cheverall et al. 2023](#)): we choose the number of components that optimizes the signal-to-noise (S/N) of an injected signal in the CCF matrix after subtracting the original CCF matrix (Figure 2). We then weight the data by the variance in each wavelength bin for a given night. The data from different orders are then combined into a 1D spectrum, so we can leverage the ratio of line strengths between orders.

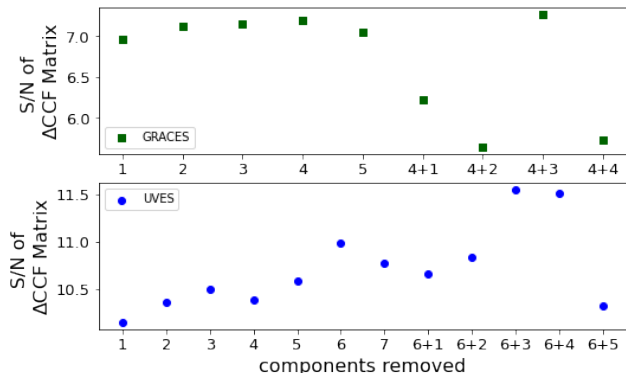


Figure 2. The S/N of the injected signal in the Δ CCF matrix as a function of components removed for GRACES (top) and UVES (bottom). The plus sign indicates additional components removed after the barycentric correction to better remove the stellar signal.

We then corrected for barycentric shift in each spectrum, as calculated with *astropy.time*, so that all the stellar signals would be aligned. We then removed any remaining signals from the star, using a second application of SVD, removing 3 components for GRACES and both UVES transits (bottom panel, figure 1). This is needed in wavelength regions with strong stellar lines, because the stellar signal moves by over ~ 500 m/s due to the barycentric shift during our observations. The improvement is seen in the re-

covery of the injected signal in the Δ CCF matrix (Figure 2).

We do not use the entire wavelength range in our final calculations. At many wavelengths, a given molecule may have approximately no opacity, so we would not expect to detect it even at much higher SNR. Other wavelengths have significant contamination from incomplete removal of telluric and/or stellar features. The worst stellar contamination, which in this case is around the Ca II Infrared triplet lines, are masked out, as are the O₂ telluric bands. For CrH, we concentrated on a bandhead at 860 nm. For both GRACES and UVES, the strongest lines are all in a single order. For UVES, the spectra cut off around 866 nm, so we simply use that as the endpoint. For GRACES, the data in principle goes past 950 nm, well into the H₂O telluric band. As the CrH features also get weaker as you go to longer wavelengths, we expect there would be very little signal added in a second order. Nevertheless, we did try the wavelength range from the second order (886 to 919 nm) both on its own and as one longer spectra from 860 to 919 nm. As the signal strength did not vary significantly with endpoints between 885 and 919 nm, we tried using different endpoints and chose the endpoint that maximized any detection significance. In this case, the final wavelength range for the GRACES data was 860 nm to 895 nm.

4.3. Deriving the Transmission Spectrum

We use standard methods for creating the CCF matrix to evaluate the presence of molecules in exoplanet atmospheres (e.g. [Birkby et al. 2013](#); [Rodler et al. 2013](#)). We first shift all spectra into the planetary rest frame using the equation:

$$\Delta v = k_p \sin \left(\frac{2\pi}{P} (t - t_c) \right) \quad (1)$$

where t is the date, t_c is the date of the transit midpoint, P is the period, Δv is the veloc-

ity shift, and k_p is the velocity amplitude of the planet. While in principle k_p can be calculated from stellar and planet orbital parameters, we chose to allow k_p to be a free parameter which we allow to vary between -200 and 200 km/s. Negative values for k_p , while physically unrealistic, allow us to better determine if any signals we see are false positives. The systemic velocities were chosen based on the initial pixel spacing for each spectrograph, so we sample the UVES data more finely than the GRACES data. Once shifted, we cross-correlate the spectra with the template before coadding the CCFs. This procedure was implemented using a custom code.³

4.4. CrH Model Templates

We created model CrH transmission spectra templates using the TRIDENT radiative transfer code (MacDonald & Lewis 2022), which employs the CrH line list from Burrows et al. (2002). Since this is an old line list, we validated it by cross-correlating our template with a high-resolution, optical spectrum of a very low-mass, cold star (Teegarden’s Star, M8) from CARMENES DR1 (Ribas et al. 2023). Very low-mass stars and warmer brown dwarfs exhibit CrH absorption starting at 860 nm (e.g. Kirkpatrick et al. 1999). In Figure 3, we plot these CCFs, which show a clear detection of CrH in the orders where we would expect to see CrH in a very low-mass star or brown dwarf.

We next created a grid of templates with isothermal temperatures from 1000 to 2200 K in increments of 400 K and volume mixing ratios (VMR) from $\log_{10}(\text{VMR}) = -6$ to -10 in increments of 1 dex. Each model atmosphere consists of 100 layers spaced uniformly in log-pressure from 10^{-9} to 100 bar. The original high-resolution model transmission spectra were computed at $\Delta\nu = 0.01 \text{ cm}^{-1}$ ($R = 10^6$ at $1 \mu\text{m}$)

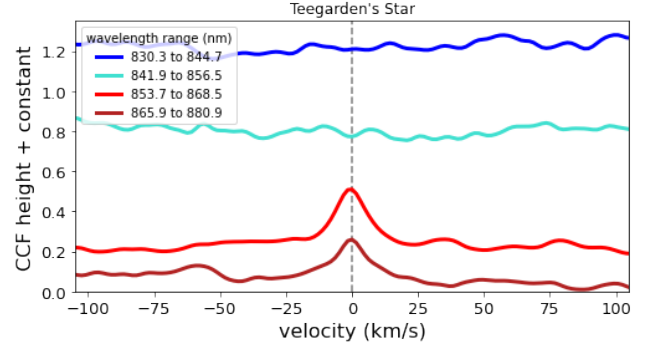


Figure 3. Cross-correlating our template with the spectra of a very low-mass star yields a clear signal in orders where CrH is expected to be present (red lines, covering wavelengths longer than 860 nm) and not the orders where it would not be present (blue lines).

and subsequently resampled to the respective resolutions of the two spectrographs, resulting in two sets of grids. We first multiplied the templates by -1, so that a detection of atmospheric absorption results in a positive correlation. We also subtract the mean and apply a Butterworth Filter to the template, as in Herman et al. (2022), to mimic the effect of the SVD on the template itself. Figure 4 shows the original version and the filtered version of the best-fit CrH template for the GRACES data. We tried using solely the 860 nm CrH band, as well as both the 764 nm and the 860 nm bands. However, as the 764 band has significant telluric contamination, we used only the 860 nm band in the final analysis (Figure 4).

5. RESULTS

5.1. CCF Matrix

We initially tried the template with grid values closest to those in Braam et al. (2021), i.e., for an isothermal temperature of 1400 K and a VMR of 10^{-8} . In the GRACES data, we find evidence of CrH at a 3.9σ level (Figure 5, top), consistent with the results from Braam et al. (2021). Our S/N is calculated by dividing the strength of the CCF by the standard deviation of the CCF matrix away from the detection.

³ <https://github.com/laurafflagg/combine-and-xcor>

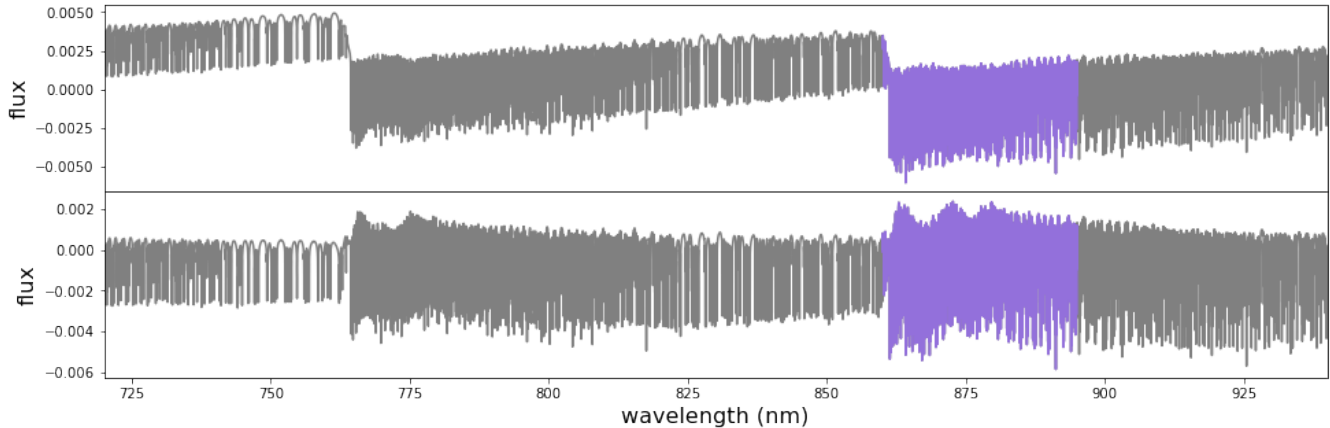


Figure 4. The original (top) and filtered CrH template (bottom). The wavelength range use, chosen because of the relatively strong CrH lines with minimal telluric contamination, is highlighted in purple.

The two UVES transits (Figure 5, middle and bottom) independently confirm evidence of CrH at 3.7σ and 3.6σ , respectively. Combining both UVES transits yields a 4.2σ CrH detection.

All other templates with different CrH abundances or atmospheric temperatures yielded similar results. We find peak strengths within 1σ of the default parameters in the CCF matrix, likely because the template does not change enough to impact the CCF. This is especially true given that the data are noisy. Consequently, our final analysis proceeded with the initial template parameters.

The location of the peak is not exactly the same for all three nights. This is not uncommon as previous studies at high resolution have seen similar discrepancies in the peak location (e.g. Merritt et al. 2021; Bello-Arufe et al. 2022; Sánchez-López et al. 2022). For a symmetric planet with no signatures of winds, we expect the peak to be at $k_p=148.0$ km/s and $v_{sys}=-0.3$ km/s. At that location, the GRACES data has dropped by $\sim 2.3\sigma$ while the UVES data has dropped by 0.8σ . These are large enough differences — especially for the GRACES data — that random noise is unlikely to be the only cause. Possible additional reasons include: 1) systematic issues, which we address with out-of-transit random sampling in Section 5.2; 2) varying SNR through the night, which will result in

an offset if the planet is not completely symmetric; 3) an incorrect ephemeris, which can result in shifting signals by several km/s in v_{sys} and 10s of km/s in k_p (Meziani et al., in prep); or 4) an asymmetric planetary signal induced because the planetary atmosphere itself is not symmetric. Since we do not know which cause is responsible, we cannot correct for it.

5.2. Bootstrap Sampling of Out-of-Transit Spectra

To confirm the significance of our detection, we evaluated the CCF signal in another manner. We use OoT spectra to model the systematic and random noise as in Esteves et al. (2017); Deibert et al. (2019). We did this twice, once for the GRACES data and once for both UVES transits. For each of 20,000 iterations, we randomly chose the same number of OoT transits frames to correspond with each in-transit phase (89 for GRACES and 154 total between the two transits for UVES). We treated that set of spectra as if they were the observed spectra and created a simulated transit spectrum and then a CCF at $k_p=148.0$ km/s, the expected k_p value for this planet (Table 1). We then compared the simulated CCFs to the actual CCF. If the signal we detected in Section 5.1 is real, then it should be stronger than the vast majority of our simulated CCFs. Because of the

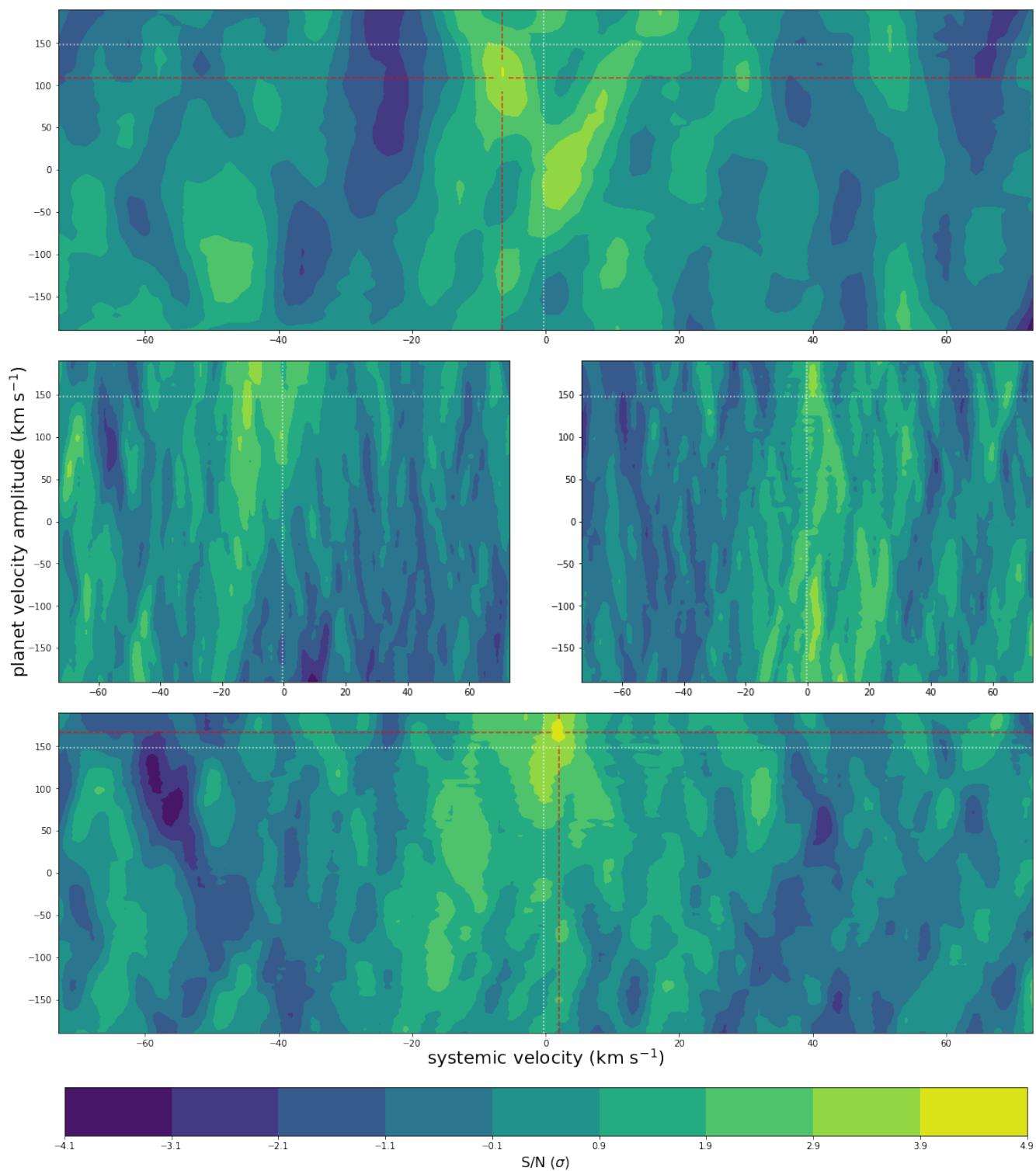


Figure 5. The CCF matrices from GRACES (top), the 1st transit with UVES (middle, left), the 2nd transit with UVES (middle, right), and both UVES transits combined (bottom). For the three transits, we detect CrH at a 3.9 , 3.7 , and 3.6σ level, respectively, while CrH is detected at a 4.2σ level for the UVES combined data set. The white dashed lines, indicating the systemic velocity of the system and the expected velocity amplitude of the planet (Table 1), cross at the expected location of the planet’s signal. The red lines indicate the peaks’ center positions.

uncertainty on v_{sys} plus the fact we fixed k_p , we allowed v_{sys} to be slightly offset from the measured v_{sys} .

We plot the results in Figure 6; the left column is for GRACES data, while the right column is for UVES data. In all four panels, the purple line is the actual CCF at the predicted k_p . The shaded regions represent the 99% region and the 99.9% region. On the top row, we plot the raw CCF values, which shows the nature of the systematics for each instrument, while the bottom row shows the CCF values with the median from the bootstrap sample at each specific v_{sys} subtracted. The GRACES maximum is above all but 99.995 % of its bootstrap sample, while the UVES maximum is above 99.97 % of its bootstrap sample. Assuming a Gaussian distribution, we used *scipy.stats.norm.ppf* to convert the one-sided probabilities into z-scores, resulting in values of ~ 3.9 and $\sim 3.5\sigma$ significance, respectively. While not identical to the numbers we calculated in Section 5.1, both are well within 1σ , showing that systematics from the spectrographs likely did not contribute much to the signals. Since these data sets can be assumed to be independent (i.e., taken on different dates, at different barycentric shifts, and with different instruments, with the caveat that unknown astrophysical systematics could create correlated noise in both data sets), we can simply multiply the probabilities to get a combined probability of 1 in ~ 80 million. Assuming a Gaussian distribution, this would be equivalent to a $\sim 5.6\sigma$ detection, confirming that we see a real signal of CrH in WASP-31b’s atmosphere.

6. CONCLUSIONS

Our detection of CrH — along with the 3.3σ evidence reported by Braam et al. (2021) at low spectral resolution — makes WASP-31b the first exoplanet with confirmed evidence of not just CrH, but any metal hydride. Moreover, our study represents the first detection of a metal

hydride at high spectral resolution in an exoplanet atmosphere.

Our results highlight a promising new window into hot Jupiter atmospheres offered by high-resolution observations. Spectral signatures of molecules like CrH are far more distinct and robust at high-resolution than at low-resolution, especially those with a low SNR. Basic templates can be created readily, so quick checks for less commonly considered species like CrH are straightforward and more computationally feasible than running a full retrieval, as is typically done for low-resolution transit spectra. As seen with UVES data in this paper and in Gibson et al. (2019), high-resolution data can easily distinguish between potassium and CrH, even though CrH has a bandhead only 2 nm from one of the most prominent potassium features.

While WASP-31b is the first exoplanet with a confirmed detection of CrH, it will undoubtedly not be the last. Detecting CrH in a single planet is merely the first step in potentially using CrH to characterize exoplanet atmospheres in a similar manner to brown dwarfs. While we are close to the limit of what is possible for characterizing CrH with ground-based, high-resolution spectroscopy today, CrH should be a viable target for exoplanets observed with JWST and the next generation of ground-based telescopes.

7. ACKNOWLEDGMENTS

Thanks to the anonymous referee for their helpful comments. We would also like to thank the very helpful team at Gemini-North, particularly Teo Mocnik, for their assistance preparing and acquiring the observations. RJ acknowledges support of a Rockefeller Foundation Belagio Center residency.

This work was enabled by observations made from the Gemini North telescope, located within the Maunakea Science Reserve and adjacent to the summit of Maunakea. We are grateful for the privilege of observing the universe

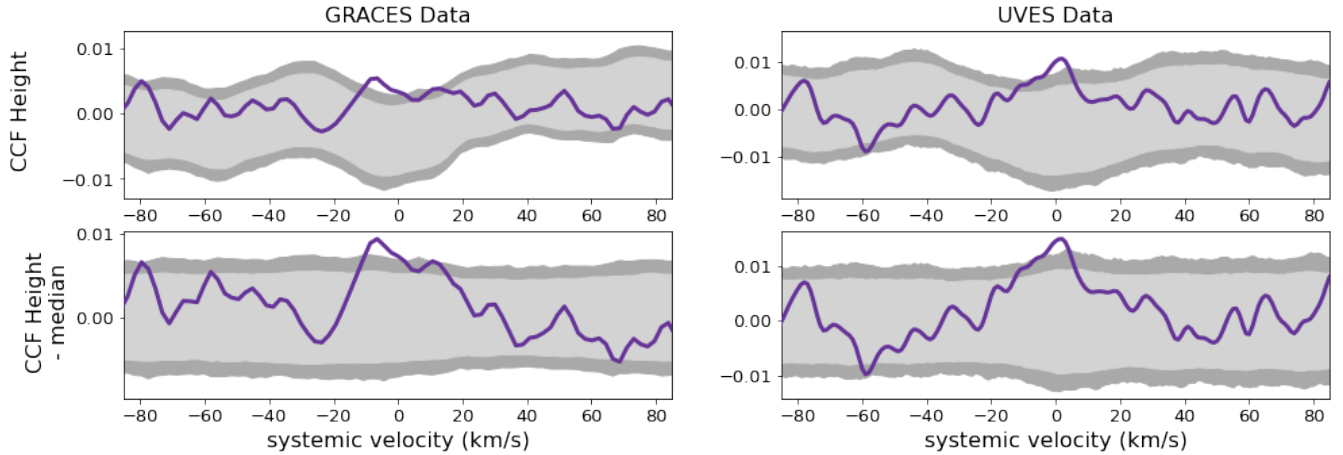


Figure 6. The CCFs at the predicted k_p (in purple) for WASP-31b along with the 99% and 99.9% ranges for the bootstrap sampling, with GRACES on the left and UVES on the right. On the top row, we plot the raw CCF values, which shows the nature of the systematics for each instrument, while the bottom row shows the CCF values with the median from the bootstrap sample at each specific v_{sys} subtracted. Assuming a Gaussian distribution, these are equivalent to 3.9σ and 3.5σ detection respectively on their own, and a 5.6σ detection when the probabilities are combined.

from a place that is unique in both its astronomical quality and its cultural significance.

This research has made use of the VizieR catalogue access tool, CDS, Strasbourg, France. The original description of the VizieR service was published by Wenger et al. (2000). This research has made use of the SIMBAD database, operated at CDS, Strasbourg, France. This research has made use of the Planetary Systems Composite Parameters Table at the NASA Exoplanet Archive (NASA Exoplanet Archive 2021), which is operated by the California Institute of Technology, under contract with the National Aeronautics and Space Administration under the Exoplanet Exploration Program.

Facility: Gemini:Gillett, VLT:Kueyen, TESS, Exoplanet Archive

Software: SpecTres (Carnall 2017), NumPy (Oliphant 2006; Van Der Walt et al. 2011), Pandas (pandas development team 2020), Matplotlib (Hunter 2007), astropy (Collaboration et al. 2013), scipy (Virtanen et al. 2020)

REFERENCES

- Anderson, D. R., Collier Cameron, A., Hellier, C., et al. 2011, *Astronomy and Astrophysics*, 531, A60
- Barstow, J. K., Aigrain, S., Irwin, P. G. J., & Sing, D. K. 2017, *The Astrophysical Journal*, 834, 50
- Bello-Arufe, A., Cabot, S. H. C., Mendonça, J. M., Buchhave, L. A., & Rathcke, A. D. 2022, *The Astronomical Journal*, 163, 96
- Birkby, J. L., de Kok, R. J., Brogi, M., et al. 2013, *Monthly Notices of the Royal Astronomical Society*, 436, L35
- Bonomo, A. S., Desidera, S., Benatti, S., et al. 2017, *Astronomy and Astrophysics*, 602, A107
- Braam, M., van der Tak, F. F. S., Chubb, K. L., & Min, M. 2021, *Astronomy and Astrophysics*, 646, A17
- Brogi, M., Snellen, I. A. G., de Kok, R. J., et al. 2013, *The Astrophysical Journal*, 767, 27
- Brown, D. J. A., Cameron, A. C., Anderson, D. R., et al. 2012, *Monthly Notices of the Royal Astronomical Society*, 423, 1503
- Burrows, A., Ram, R. S., Bernath, P., Sharp, C. M., & Milsom, J. A. 2002, *The Astrophysical Journal*, 577, 986
- Carnall, A. C. 2017, arXiv:1705.05165 [astro-ph]. <http://ascl.net/1705.05165>
- Cheverall, C. J., Madhusudhan, N., & Holmberg, M. 2023, *Monthly Notices of the Royal Astronomical Society*, 522, 661
- Claret, A. 2017, *Astronomy & Astrophysics*, 600, A30
- Collaboration, A., Robitaille, T. P., Tollerud, E. J., et al. 2013, *Astronomy and Astrophysics*, 558
- Deibert, E. K., de Mooij, E. J. W., Jayawardhana, R., et al. 2019, *The Astronomical Journal*, 157, 58
- . 2021, *The Astrophysical Journal*, 919, L15
- Eastman, J., Gaudi, B. S., & Agol, E. 2013, *Publications of the Astronomical Society of the Pacific*, 125, 83
- Esteves, L. J., de Mooij, E. J. W., Jayawardhana, R., Watson, C., & de Kok, R. 2017, *The Astronomical Journal*, 153, 268
- Flagg, L., Johns-Krull, C. M., Nofi, L., et al. 2019, *The Astrophysical Journal Letters*, 878, L37
- Ford, E. B. 2006, *The Astrophysical Journal*, 642, 505
- Fortney, J. J., Lodders, K., Marley, M. S., & Freedman, R. S. 2008, *The Astrophysical Journal*, 678, 1419
- Gaia Collaboration, Brown, A. G. A., Vallenari, A., et al. 2018, *Astronomy and Astrophysics*, 616, A1
- Gandhi, S., & Madhusudhan, N. 2019, *Monthly Notices of the Royal Astronomical Society*, 485, 5817
- Gelman, A., & Rubin, D. B. 1992, *Statistical Science*, 7, 457
- Gibson, N. P., de Mooij, E. J. W., Evans, T. M., et al. 2019, *Monthly Notices of the Royal Astronomical Society*, 482, 606
- Gibson, N. P., Nikolov, N., Sing, D. K., et al. 2017, *Monthly Notices of the Royal Astronomical Society*, 467, 4591
- Herman, M. K., de Mooij, E. J. W., Jayawardhana, R., & Brogi, M. 2020, *The Astronomical Journal*, 160, 93
- Herman, M. K., de Mooij, E. J. W., Nugroho, S. K., Gibson, N. P., & Jayawardhana, R. 2022, *The Astronomical Journal*, 163, 248
- Hunter, J. D. 2007, *Computing in Science & Engineering*, 9, 90
- Kesseli, A. Y., Snellen, I. A. G., Alonso-Floriano, F. J., Mollière, P., & Serindag, D. B. 2020, *The Astronomical Journal*, 160, 228
- Kirkpatrick, J. D., Reid, I. N., Liebert, J., et al. 1999, *The Astrophysical Journal*, 519, 802
- Line, M. R., Brogi, M., Bean, J. L., et al. 2021, *Nature*, 598, 580
- Lockwood, A. C., Johnson, J. A., Bender, C. F., et al. 2014, *The Astrophysical Journal Letters*, 783, L29
- MacDonald, R. J., & Lewis, N. K. 2022, *The Astrophysical Journal*, 929, 20
- MacDonald, R. J., & Madhusudhan, N. 2017, *The Astrophysical Journal Letters*, 850, L15
- . 2019, *Monthly Notices of the Royal Astronomical Society*, 486, 1292
- Mandel, K., & Agol, E. 2002, *The Astrophysical Journal*, 580, L171
- Martín, E. L., Delfosse, X., Basri, G., et al. 1999, *The Astronomical Journal*, 118, 2466
- Martioli, E., Teple, D., Manset, N., et al. 2012, 8451, 84512B

- McGruder, C. D., López-Morales, M., Espinoza, N., et al. 2020, *The Astronomical Journal*, 160, 230
- Merritt, S. R., Gibson, N. P., Nugroho, S. K., et al. 2021, *Monthly Notices of the Royal Astronomical Society*, 506, 3853
- NASA Exoplanet Archive. 2021, Planetary Systems Composite Parameters, Last Access: 20XX-YY-ZZ, NExScI-Caltech/IPAC, doi: [10.26133/NEA13](https://doi.org/10.26133/NEA13)
- Nugroho, S. K., Kawahara, H., Masuda, K., et al. 2017, *The Astronomical Journal*, 154, 221
- Oliphant, T. E. 2006 (Trelgol Publishing USA)
- pandas development team, T. 2020, Zenodo
- Pearson, K. A., Turner, J. D., & Sagan, T. G. 2014, *New Astronomy*, 27, 102
- Rathcke, A. D., MacDonald, R. J., Barstow, J. K., et al. 2021, *The Astronomical Journal*, 162, 138
- Reid, I. N., Hawley, S. L., & Gizis, J. E. 1995, *The Astronomical Journal*, 110, 1838
- Ribas, I., Reiners, A., Zechmeister, M., et al. 2023, *Astronomy and Astrophysics*, 670, A139
- Rodler, F., Kürster, M., & Barnes, J. R. 2013, *Monthly Notices of the Royal Astronomical Society*, 432, 1980
- Sánchez-López, A., Landman, R., Mollière, P., et al. 2022, *Astronomy and Astrophysics*, 661, A78
- Sing, D. K., Wakeford, H. R., Showman, A. P., et al. 2015, *Monthly Notices of the Royal Astronomical Society*, 446, 2428
- Skaf, N., Bieger, M. F., Edwards, B., et al. 2020, *The Astronomical Journal*, 160, 109
- Sotzen, K. S., Stevenson, K. B., Sing, D. K., et al. 2020, *The Astronomical Journal*, 159, 5
- Spring, E. F., Birkby, J. L., Pino, L., et al. 2022, *Astronomy and Astrophysics*, 659, A121
- Turner, J. D., Flagg, L., Ridden-Harper, A., & Jayawardhana, R. 2022, *The Astronomical Journal*, 163, 281
- Turner, J. D., Ridden-Harper, A., & Jayawardhana, R. 2021, *The Astronomical Journal*, 161, 72
- Turner, J. D., Leiter, R. M., Biddle, L. I., et al. 2017, *Monthly Notices of the Royal Astronomical Society*, 472, 3871
- Van Der Walt, S., Colbert, S. C., & Varoquaux, G. 2011, *Computing in Science & Engineering*, 13, 22
- Virtanen, P., Gommers, R., Oliphant, T. E., et al. 2020, *Nature Methods*, 17, 261
- Visscher, C., Lodders, K., & Fegley, Jr., B. 2010, *The Astrophysical Journal*, 716, 1060
- Welbanks, L., Madhusudhan, N., Allard, N. F., et al. 2019, *The Astrophysical Journal*, 887, L20
- Wenger, M., Ochsenbein, F., Egret, D., et al. 2000, *Astronomy and Astrophysics Supplement Series*, 143, 9
- Zacharias, N., Finch, C. T., Girard, T. M., et al. 2013, *The Astronomical Journal*, 145, 44

APPENDIX

A. TESS TRANSIT TIMINGS

The mid-transit time for each TESS transit fit can be found in Table A1.

Table A1. Individual TESS (Sectors 9 and 36) mid-transit times for WASP-31b derived using EXOMOP

Epoch	T_c (BJD _{TDB})	T_c 1σ Error (BJD _{TDB})
785	2458547.4879012	0.00066
786	2458550.8946979	0.00060
787	2458554.2997179	0.00061
788	2458557.7055964	0.00068
789	2458561.1115885	0.00063
1001	2459283.1594180	0.00061
1002	2459286.5652727	0.00070
1003	2459289.9714827	0.00062
1005	2459296.7833610	0.00071
1006	2459300.1886769	0.00065
1007	2459303.5956452	0.00077